

Joint gravitational wave detection by TianQin and LISA

Alejandro Torres-Orjuela¹

Department of Physics, The University of Hong Kong, Pokfulam Road, Hong Kong,
 atorreso@hku.hk

Abstract. We study the detection accuracy of double white dwarfs (DWDs), stellar-mass black hole binaries (SBHBs), light and heavy intermediate mass ratio inspirals (IMRIs), extreme mass ratio inspirals (EMRIs), massive black hole binaries (MBHBs), and the stochastic gravitational wave background (SGWB) of astronomical origin for TianQin, LISA, and joint detection. We use a Fisher matrix analysis and consider for each source the averaged detection accuracy over a realistic range of parameters. We find that on average TianQin obtains more accurate parameter estimation for DWDs and light IMRIs, LISA for heavy IMRIs, EMRIs, MBHBs, and the galactic foreground of the SGWB, and both contribute similarly to the detection of SBHBs and the extra-galactic SGWB. Nevertheless, for all sources joint detection allows setting tighter constraints on most parameters highlighting its importance for future detection.

Keywords: gravitational waves, gravitational wave detection, space-based detectors

1 Introduction

Gravitational wave (GW) detection has opened a new window to study compact objects [1,2,3] although it is currently restricted to the high-frequency band above 1 Hz covered by ground-based laser interferometry detectors LIGO, Virgo, and KAGRA [4,5,6] and the nHz band accessible through pulsar timing arrays [7,8,9,10,11,12]. The detectable spectrum will be expanded in the mid-2030s to the low-frequency (mHz) band by space-based laser interferometry detectors TianQin, LISA, and Taiji [13,14,15] while the intermediate band (dHz) will be opened by space-based laser interferometry detectors like DECIGO [16], ground-based and space-based atom interferometry detectors like AION, ZAIGA, and AEDGE [17,18,19] as well as lunar GW detectors like LGWA [20] in coming years.

TianQin and LISA are two space-based laser interferometer detectors with a similar design but differ in key aspects. Due to the differences in their design, TianQin and LISA can detect the same sources but obtain different accuracies. These sources include double white dwarfs (DWDs) which are the most abundant class of compact stellar mass binaries in our galaxy [21,22,23], stellar-mass

black hole binaries (SBHBs) formed through co-evolving massive stars [24,25,26] or dynamical assembling in dense stellar systems [27,28,29], light intermediate mass ratio inspirals (IMRIs) formed by a stellar-mass black hole (BH) orbiting an intermediate-mass BH (IMBH) [30,31,32], heavy IMRIs formed by an IMBH orbiting a massive BH [33,34,35], extreme mass ratio inspirals (EMRIs) formed by a small compact object inspiraling into a MBH [36,37], MBH binaries (MBHBs) residing in the center of galaxies [38,39,40], and the stochastic GW background (SGWB) resulting from the combination of a multitude of unresolved binaries [41,42,43].

We study the detection of astrophysical GW sources by TianQin, LISA, and joint detection using a Fisher matrix analysis [44,45,46]. The inverse of the Fisher Matrix $C = F^{-1}$ is a linear estimate of the measurement errors that asymptotes the true error in the limit of high signal-to-noise ratio. The detection accuracy of the joint detection is obtained by combining the results of the two independent detectors $F_{\text{Joint}} = F_{\text{TianQin}} + F_{\text{LISA}}$ and then inverting F_{Joint} . We focus on comparing the averaged detection accuracy of TianQin, LISA, and joint detection. However, the detection accuracy of a parameter can vary significantly depending on its specific value. Therefore, the results shown here shall only give an idea of the detection accuracy for the different detection scenarios and we refer the reader to Ref. [45] for more details. Moreover, when calculating the errors over the parameter range we only vary the considered parameter and fix the other parameters to fiducial values.

2 Detection by TianQin, LISA, and joint detection

2.1 Double white dwarfs

The parameters we consider for DWDs are the luminosity distance D_L , the chirp mass M_c , the inclination of the orbit relative to the line-of-sight ι , the orbital period of the binary P , and the sky localization Ω . We consider the sky localization error as a function of the declination dec and the right ascension RA where one is fixed while the other is varied. The fiducial values, the parameter ranges considered as well as the average errors are shown in Tab. 1. Note that the average errors for dec and RA refer to the sky localization error $\Delta\Omega$ as a function of these two parameters and are given in units of deg^2 . We see on the left-hand side of Fig. 1 that TianQin constrains D_L , M_c , ι , and Ω_{RA} better than LISA while LISA can set tighter constraints than TianQin for P and Ω_{dec} . Therefore, we find that although the detection of single parameters of a DWD might be dominated by one of the two detectors, joint detection yields significantly better results when studying all parameters combined. Note that as in real detection, all parameters are measured at the same time the improvements from joint detection are even more significant than they appear here. Last, we point out that the relatively big error in Ω_{dec} compared to Ω_{RA} for TianQin can be attributed to the particular choice of fiducial parameters and similar accuracies to those of Ω_{RA} can be expected for most sources.

Table 1. The fiducial values, the parameter ranges, and the averaged absolute errors in TianQin, LISA, and joint detection for DWDs.

	D_L [kpc]	M_c [M_\odot]	ι [π]	P [s]	dec	RA
Fiducial	8.5	0.25	1/3	200	-5.6°	17.8^h
Range	0.01-50	0.1-1.25	0-0.5	10-500	-90° - $+90^\circ$	0^h - 24^h
TianQin	1.2	4.6×10^{-4}	5.3×10^{-2}	8.9×10^{-4}	1.7	2.1×10^{-3}
LISA	1.8	6.1×10^{-4}	1.1×10^{-1}	2.5×10^{-4}	2.6×10^{-1}	1.3×10^{-2}
Joint	8.7×10^{-1}	3.6×10^{-4}	4.2×10^{-2}	2.4×10^{-4}	2.0×10^{-1}	1.5×10^{-4}

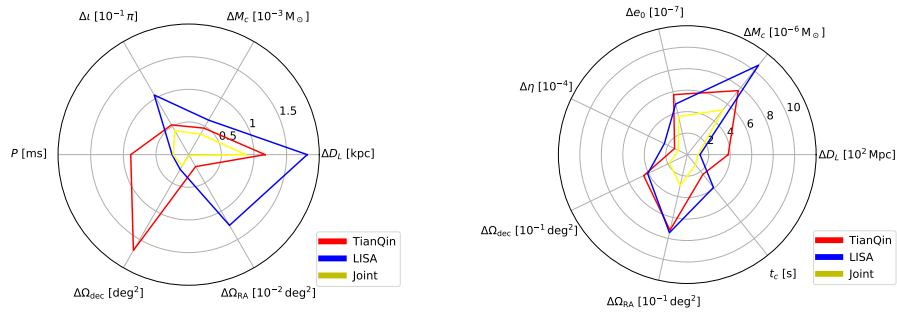


Fig. 1. The averaged absolute error for the parameters of DWDs (left) and SMBHs (right) measured by TianQin (red), LISA (blue), and joint detection (yellow).

2.2 Stellar-mass black hole binaries

For SBHBs, we consider D_L , M_c , the binary's eccentricity at 10 mHz e_0 , the symmetric mass ratio η , Ω , and time to coalescence t_c . Their fiducial values, parameter range, and the averaged absolute errors in TianQin, LISA, and joint detection can be found in Tab. 2. From the right side of Fig. 1 we see that M_c , η , and t_c are constrained better by TianQin while D_L and e_0 have smaller errors in LISA. Moreover, we see that Ω_{dec} and Ω_{RA} are constrained to a similar level by both detectors, and the small difference can be mainly attributed to the particular choice of fiducial values. In general, all parameters are constrained to a similar level by TianQin and LISA leading to a significant improvement in joint detection - in particular, for Ω , e_0 , and M_c .

Table 2. The fiducial values, the parameter ranges, and the averaged absolute errors in TianQin, LISA, and joint detection for SBHBs.

	D_L [Mpc]	M_c [M_\odot]	e_0	η	dec	RA	t_c
Fiducial	200	50	0.05	0.125	+30°	12 ^h	2.5 yr
Range	100-530	3.5-100	0.01-0.1	0.001-0.25	0°-+90°	0 ^h -24 ^h	1 yr-5 yr
TianQin	380	7.6×10^{-6}	5.7×10^{-7}	1.3×10^{-4}	4.5×10^{-1}	7.2×10^{-1}	2.3 s
LISA	110	1.1×10^{-5}	4.8×10^{-7}	2.4×10^{-4}	4.1×10^{-1}	7.5×10^{-1}	3.9 s
Joint	100	5.3×10^{-6}	3.6×10^{-7}	9.2×10^{-5}	1.8×10^{-1}	2.9×10^{-1}	1.2 s

2.3 Light intermediate mass ratio inspirals

We consider D_L , the total mass M , the mass ratio q , ι , and Ω as the parameters of light IMRIs, where the fiducial values and the parameter range used are shown in Tab. 3. The averaged absolute errors for TianQin, LISA, and joint detection can be found in the same table. The left-hand side of Fig. 2 shows the averaged detection error for light IMRIs. We see that the detection accuracy of TianQin is significantly better than the detection accuracy of LISA; often differing by almost an order of magnitude. Therefore, the accuracy of joint detection is dominated by TianQin but LISA can contribute to an improved detection of Ω and M .

2.4 Heavy intermediate mass ratio inspirals

For heavy IMRIs, we consider the same parameters as for a light IMRI, namely D_L , M , q , ι , and Ω . In Tab. 4 we show the fiducial values, the parameter range, and the averaged detection error for TianQin, LISA, and joint detection. We, further, see on the right side of Fig. 2 that the detection accuracy in LISA is significantly better than TianQin's although the difference is less than one order

Table 3. The fiducial values and the parameter ranges as well as the averaged detection errors in TianQin, LISA, and joint detection for light IMRIs.

Parameter	D_L [Mpc]	M [M_\odot]	q	ι [π]	dec	RA
Fiducial	1	5000	100	1/3	0°	12^h
Range	0.001-100	$550-10^5$	10-5000	0-0.5	$0^\circ-+90^\circ$	0^h-24^h
TianQin	2.6	35	5.1×10^{-1}	1.9×10^{-3}	2.4×10^{-4}	3.6×10^{-4}
LISA	15.5	169	3.9	1.2×10^{-2}	3.9×10^{-2}	1.7×10^{-2}
Joint	2.6	32	5.1×10^{-1}	1.9×10^{-3}	1.3×10^{-4}	2.4×10^{-4}

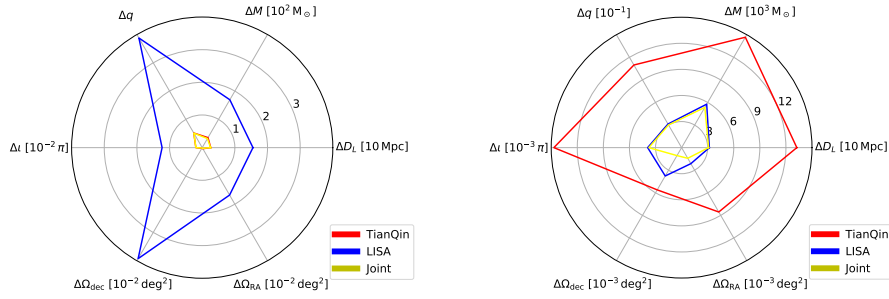


Fig. 2. The averaged absolute error for the parameters of light IMRIs (left) and heavy IMRIs (right) measured by TianQin (red), LISA (blue), and joint detection (yellow).

of magnitude. Therefore, the constraints set by the joint detection are similar to those of LISA for D_L , M , q , and ι . For Ω the detection accuracy of the joint detection is also dominated by LISA but TianQin can considerably contribute to an improved measurement.

Table 4. The fiducial values, the parameter ranges, and the averaged detection errors for heavy IMRIs by TianQin, LISA, and joint detection.

Parameter	D_L [Mpc]	M [M_\odot]	q	ι [π]	dec	RA
Fiducial	30	10^6	100	1/3	0°	12^h
Range	1-1000	10^5 - $10^{6.2}$	10-5000	0-0.5	0° - $+90^\circ$	0^h - 24^h
TianQin	133	1.5×10^4	1.1	1.5×10^{-2}	5.6×10^{-3}	8.4×10^{-3}
LISA	32	5.8×10^3	3.1×10^{-1}	3.9×10^{-3}	3.7×10^{-3}	2.1×10^{-3}
Joint	31	5.3×10^3	3.0×10^{-1}	3.8×10^{-3}	1.1×10^{-3}	1.4×10^{-3}

2.5 Extreme mass ratio inspirals

The parameters we study for an EMRI are ΔD_L , the mass of the MBH M_1 , the eccentricity at merger e_m , the spin of the primary BH s , and Ω . We show their fiducial values, the parameter range considered, and the averaged detection errors by TianQin, LISA, and joint detection in Tab. 5. Moreover, we set the mass of the SBH orbiting the MBH to $10 M_\odot$. The left-hand side of Fig. 3 shows that the detection accuracy of LISA is significantly better than the detection accuracy of TianQin but differs by less than one order of magnitude. Nevertheless, TianQin can contribute to slightly better constraints in the joint detection for D_L , M_1 , e_m , and s . Only the accuracy of Ω in the joint detection is completely dominated by LISA which, however, can be partially attributed to the fiducial values assumed.

Table 5. The fiducial values, the parameter ranges, and the averaged absolute errors of the parameter in TianQin, LISA, and joint detection for EMRIs.

Parameter	D_L [Gpc]	M_1 [M_\odot]	e_m	s	dec	RA
Fiducial	1	10^6	0.1	0.98	$+30^\circ$	0^h
Range	0.01-10	10^5 - 10^7	0.002-0.5	0.8-0.998	-90° - $+90^\circ$	0^h - 24^h
TianQin	5.0×10^{-1}	6.5	7.9×10^{-5}	9.4×10^{-5}	1.8×10^{-1}	2.9×10^{-1}
LISA	1.6×10^{-1}	3.0	3.0×10^{-5}	3.0×10^{-5}	1.7×10^{-2}	1.7×10^{-2}
Joint	1.5×10^{-1}	2.7	2.8×10^{-5}	2.9×10^{-5}	1.7×10^{-2}	1.7×10^{-2}

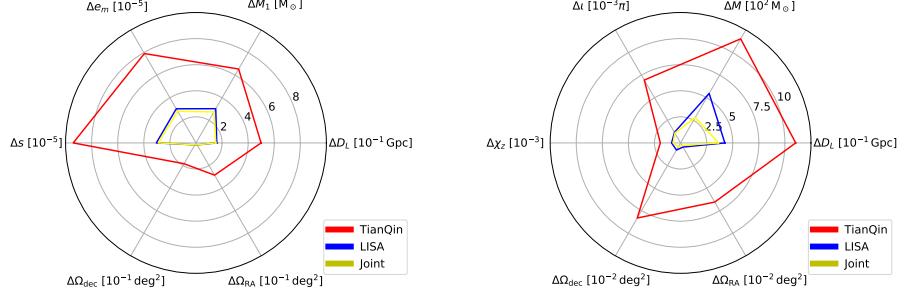


Fig. 3. The averaged absolute errors TianQin (red), LISA (blue), and joint detection (yellow) measure for the parameters of EMRI s(left) and MBHBs (right).

2.6 Massive black hole binaries

We consider D_L , M , ι , the effective spin of the BH along the angular momentum χ_z , and Ω as the parameters of MBHBs. We assume the components of the binary to be of equal mass and thus the effective spin refers to any of the two MBHs. Tab. 6 shows the fiducial values and the parameter ranges considered as well as the averaged detection error for TianQin, LISA, and joint detection. On the right-hand side of Fig. 3, we see that LISA’s detection error is smaller than TianQin’s by a factor of two to three for most parameters. Only for Ω , the difference is more significant being of more than one order of magnitude. Therefore, the contribution by TianQin to the joint detection for Ω is small but the constraints on D_L and M are significantly improved in joint detection compared to LISA alone.

Table 6. The fiducial values and the parameter ranges as well as TianQin’s, LISA’s, and joint detection’s averaged absolute errors for MBHBs.

Parameter	D_L [Gpc]	M [M_\odot]	ι [π]	χ_z	dec	RA
Fiducial	10.5	4×10^6	1/3	0.5	$+45^\circ$	1.95^h
Range	0.5-50	10^4 - 10^7	0-1	0.04-0.96	-90° - $+90^\circ$	0^h - 24^h
TianQin	1.1	1.2×10^3	7.0×10^{-3}	1.9×10^{-3}	8.3×10^{-2}	6.5×10^{-2}
LISA	4.2×10^{-1}	5.5×10^2	1.2×10^{-3}	8.6×10^{-4}	7.9×10^{-3}	4.6×10^{-3}
Joint	3.6×10^{-1}	2.8×10^2	1.1×10^{-3}	7.1×10^{-4}	4.2×10^{-3}	2.8×10^{-3}

2.7 Stochastic gravitational wave background

The energy spectrum density of the SGWB can be parametrized as

$$\Omega_{\text{GW}} = \Omega_0 \left(\frac{f}{f_{\text{ref}}} \right)^{\alpha_0} + \Omega_1 \left(\frac{f}{f_{\text{ref}}} \right)^{\alpha_1} \left[1 + 0.75 \left(\frac{f}{f_{\text{ref}}} \right)^{\Delta} \right]^{(\alpha_2 - \alpha_1)/\Delta}, \quad (1)$$

where the first term represents the background formed by extra-galactic binaries [47,48,49] and the second term describes the foreground produced by Galactic DWDs [50]. Ω_0 is the amplitude level of the background at the reference frequency f_{ref} and $\alpha_0 = 2/3$ is the spectral index for a background of binaries. Moreover, we set $\Omega_1 = 1 \times 10^{-6.94}$, $\alpha_1 = 3.64$, $\alpha_2 = -3.95$, and $\Delta = 0.75$. For the dimensionless energy density of the SGWB, we consider the range $10^{-12} \leq \Omega_{\text{GW}} \leq 10^{-9}$ in accordance with the results of the LIGO-Virgo-KAGRA Collaboration [51].

We see in Fig. 4 that the parameters of the background Ω_0 and α_0 are constrained slightly better by LISA than by TianQin. Therefore, both contribute significantly to the joint detection of these parameters. The detection of the foreground is dominated by LISA and thus joint detection of Ω_1 , α_1 , and α_2 only improves slightly by TianQin's contribution. For the detailed averaged relative errors see Tab. 7.

Table 7. The averaged detection errors in TianQin, LISA, and joint detection for the SGWB.

Parameter	Ω_0	α_0	Ω_1	α_1	α_2
TianQin	2.0×10^{-1}	1.6×10^{-1}	1.4×10^{-1}	2.3×10^{-1}	2.1×10^{-1}
LISA	1.7×10^{-1}	1.5×10^{-1}	7.0×10^{-2}	1.1×10^{-1}	1.2×10^{-1}
Joint	1.2×10^{-1}	1.0×10^{-1}	5.5×10^{-2}	8.4×10^{-2}	9.1×10^{-2}

3 Summary

We study how accurately the parameters of DWDs, SBHBs, light and heavy IMRIs, EMRIs, MBHBs, and the SGWB formed by unresolved binaries are detected by TianQin, LISA, and joint detection. For each source, we consider a range of realistic parameters and compute the averaged detection error. We find that TianQin's detection accuracy is particularly good for DWDs and light IMRIs while LISA obtains tighter constraints for heavy IMRIs, EMRIs, MBHBs, and the galactic foreground of the SGWB. For SBHBs and the extra-galactic SGWB, TianQin and LISA obtain comparable results thus contributing similarly to joint detection. However, for all sources, joint detection yields improved

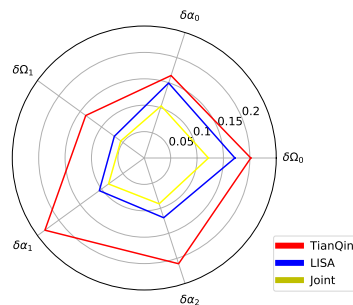


Fig. 4. The averaged relative error for the parameters of the extra-galactic background and the galactic foreground of the SGWB measured by TianQin (red), LISA (blue), and joint detection (yellow).

detection accuracies showing the importance of coordinated detections. This study focuses on the averaged detection accuracy but detection errors can vary significantly depending on the specific value of the parameter. Therefore, we refer interested readers to Ref. [45] where the detection accuracy for TianQin, LISA, and joint detection are discussed in more detail. Although the discussion in Ref. [45] is much more extensive, the topic of joint detection requires further studies to understand the potential profit of coordinated detections by TianQin and LISA.

References

1. The LIGO Scientific Collaboration and the Virgo Collaboration. GWTC-1: A Gravitational-Wave Transient Catalog of Compact Binary Mergers Observed by LIGO and Virgo during the First and Second Observing Runs. *Physical Review X*, 9(3):031040, Jul 2019.
2. The LIGO Scientific Collaboration and the Virgo Collaboration. GWTC-2: Compact Binary Coalescences Observed by LIGO and Virgo during the First Half of the Third Observing Run. *Physical Review X*, 11(2):021053, April 2021.
3. The LIGO Scientific Collaboration, the Virgo Collaboration, and the KAGRA Collaboration. GWTC-3: Compact Binary Coalescences Observed by LIGO and Virgo During the Second Part of the Third Observing Run. *arXiv e-prints*, page arXiv:2111.03606, November 2021.
4. LIGO Scientific Collaboration. Advanced LIGO. *Classical and Quantum Gravity*, 32(7):074001, April 2015.
5. T. Accadia et al. Virgo: a laser interferometer to detect gravitational waves. *Journal of Instrumentation*, 7(3):3012, March 2012.
6. Kagra Collaboration. KAGRA: 2.5 generation interferometric gravitational wave detector. *Nature Astronomy*, 3:35–40, Jan 2019.
7. R. N. Manchester and IPTA. The International Pulsar Timing Array. *Classical and Quantum Gravity*, 30(22):224010, November 2013.

8. P. B. Demorest, R. D. Ferdman, M. E. Gonzalez, D. Nice, S. Ransom, I. H. Stairs, Z. Arzoumanian, A. Brazier, S. Burke-Spolaor, S. J. Chamberlin, et al. Limits on the Stochastic Gravitational Wave Background from the North American Nanohertz Observatory for Gravitational Waves. *Astrophys. J.*, 762(2):94, January 2013.
9. R. N. Manchester, G. Hobbs, M. Bailes, W. A. Coles, W. van Straten, M. J. Keith, R. M. Shannon, N. D. R. Bhat, A. Brown, S. G. Burke-Spolaor, et al. The Parkes Pulsar Timing Array Project. *Publ. Astron. Soc. Aust.*, 30:e017, January 2013.
10. K. J. Lee. Prospects of Gravitational Wave Detection Using Pulsar Timing Array for Chinese Future Telescopes. In L. Qain and D. Li, editors, *Frontiers in Radio Astronomy and FAST Early Sciences Symposium 2015*, volume 502 of *Astronomical Society of the Pacific Conference Series*, page 19, February 2016.
11. G. Desvignes, R. N. Caballero, L. Lentati, J. P. W. Verbiest, D. J. Champion, B. W. Stappers, G. H. Janssen, P. Lazarus, S. Osłowski, S. Babak, et al. High-precision timing of 42 millisecond pulsars with the European Pulsar Timing Array. *Mon. Not. R. Astron. Soc.*, 458(3):3341–3380, May 2016.
12. Bhal Chandra Joshi, Prakash Arumugasamy, Manjari Bagchi, Debades Bandyopadhyay, Avishek Basu, Neelam Dhanda Batra, Suryarao Bethapudi, Arpita Choudhary, Kishalay De, L. Dey, et al. Precision pulsar timing with the ORT and the GMRT and its applications in pulsar astrophysics. *Journal of Astrophysics and Astronomy*, 39(4):51, August 2018.
13. Jun Luo, Li-Sheng Chen, Hui-Zong Duan, Yun-Gui Gong, Shoucun Hu, Jianghui Ji, Qi Liu, Jianwei Mei, Vadim Milyukov, Mikhail Sazhin, et al. TianQin: a spaceborne gravitational wave detector. *Classical and Quantum Gravity*, 33(3):035010, February 2016.
14. Pau Amaro-Seoane, Heather Audley, Stanislav Babak, John Baker, Enrico Barausse, Peter Bender, Emanuele Berti, Pierre Binétruy, Michael Born, Daniele Bortoluzzi, et al. Laser Interferometer Space Antenna. *arXiv e-prints*, page arXiv:1702.00786, February 2017.
15. X. Gong, Y.-K. Lau, S. Xu, P. Amaro-Seoane, S. Bai, X. Bian, Z. Cao, G. Chen, X. Chen, Y. Ding, et al. Descope of the ALIA mission. In *Journal of Physics Conference Series*, volume 610 of *Journal of Physics Conference Series*, page 012011, May 2015.
16. Seiji Kawamura, Masaki Ando, Naoki Seto, Shuichi Sato, Mitsuru Musha, Isao Kawano, Jun'ichi Yokoyama, Takahiro Tanaka, Kunihito Ioka, Tomotada Akutsu, et al. Current status of space gravitational wave antenna DECIGO and B-DECIGO. *Progress of Theoretical and Experimental Physics*, 2021(5):05A105, May 2021.
17. L. Badurina et al. AION: An Atom Interferometer Observatory and Network. *JCAP*, 05:011, 2020.
18. Ming-Sheng Zhan, Jin Wang, Wei-Tou Ni, Dong-Feng Gao, Gang Wang, Ling-Xiang He, Run-Bing Li, Lin Zhou, Xi Chen, Jia-Qi Zhong, et al. ZAIGA: Zhaoshan long-baseline atom interferometer gravitation antenna. *International Journal of Modern Physics D*, 29(4):1940005, January 2020.
19. Yousef Abou El-Neaj, Cristiano Alpigiani, Sana Amairi-Pyka, Henrique Araujo, Antun Balaz, Angelo Bassi, Lars Bathe-Peters, Baptiste Battelier, Aleksandar Belic, Elliot Bentine, et al. AEDGE: Atomic Experiment for Dark Matter and Gravity Exploration in Space. *EPJ Quantum Technology*, 7:6, March 2020.
20. Parameswaran Ajith, Pau Amaro Seoane, Manuel Arca Sedda, Riccardo Arcodia, Francesca Badaracco, et al. The Lunar Gravitational-wave Antenna: Mission Studies and Science Case. *arXiv e-prints*, page arXiv:2404.09181, April 2024.

21. G. Nelemans, L. R. Yungelson, and S. F. Portegies Zwart. The gravitational wave signal from the Galactic disk population of binaries containing two compact objects. *Astron. Astrophys.*, 375:890–898, September 2001.
22. S. Yu and C. S. Jeffery. The gravitational wave signal from diverse populations of double white dwarf binaries in the Galaxy. *Astron. Astrophys.*, 521:A85, October 2010.
23. Katelyn Breivik, Scott Coughlin, Michael Zevin, Carl L. Rodriguez, Kyle Kremer, Claire S. Ye, Jeff J. Andrews, Michael Kurkowski, Matthew C. Digman, Shane L. Larson, et al. COSMIC Variance in Binary Population Synthesis. *Astrophys. J.*, 898(1):71, July 2020.
24. Dany Vanbeveren. The evolution of massive and very massive stars in clusters. *New Astron. Rev.*, 53(1-2):27–35, May 2009.
25. Krzysztof Belczynski, Michal Dominik, Tomasz Bulik, Richard O’Shaughnessy, Chris Fryer, and Daniel E. Holz. The Effect of Metallicity on the Detection Prospects for Gravitational Waves. *Astrophys. J. Lett.*, 715(2):L138–L141, June 2010.
26. Matthias U. Kruckow, Thomas M. Tauris, Norbert Langer, Michael Kramer, and Robert G. Izzard. Progenitors of gravitational wave mergers: binary evolution with the stellar grid-based code COMBINE. *Mon. Not. R. Astron. Soc.*, 481(2):1908–1949, December 2018.
27. Simon F. Portegies Zwart and Stephen L. W. McMillan. Black Hole Mergers in the Universe. *Astrophys. J. Lett.*, 528(1):L17–L20, January 2000.
28. Kayhan Gültekin, M. Coleman Miller, and Douglas P. Hamilton. Growth of Intermediate-Mass Black Holes in Globular Clusters. *Astrophys. J.*, 616(1):221–230, November 2004.
29. Hiromichi Tagawa, Zoltán Haiman, and Bence Kocsis. Formation and Evolution of Compact-object Binaries in AGN Disks. *Astrophys. J.*, 898(1):25, July 2020.
30. Clifford M. Will. On the Rate of Detectability of Intermediate-Mass Black Hole Binaries Using LISA. *Astrophys. J.*, 611(2):1080–1083, August 2004.
31. Pau Amaro-Seoane, Jonathan R. Gair, Marc Freitag, M. Coleman Miller, Ilya Mandel, Curt J. Cutler, and Stanislav Babak. TOPICAL REVIEW: Intermediate and extreme mass-ratio inspirals—astrophysics, science applications and detection using LISA. *Classical and Quantum Gravity*, 24(17):R113–R169, September 2007.
32. Manuel Arca Sedda, Pau Amaro Seoane, and Xian Chen. Merging stellar and intermediate-mass black holes in dense clusters: implications for LIGO, LISA, and the next generation of gravitational wave detectors. *Astron. Astrophys.*, 652:A54, August 2021.
33. Prasad Basu and Sandip K. Chakrabarti. Gravitational wave emission from a companion black hole in presence of an accretion disk around a super-massive Kerr black hole. In Sandip K. Chakrabarti and Archan S. Majumdar, editors, *American Institute of Physics Conference Series*, volume 1053 of *American Institute of Physics Conference Series*, pages 33–37, October 2008.
34. Manuel Arca-Sedda and Alessia Gualandris. Gravitational wave sources from inspiralling globular clusters in the Galactic Centre and similar environments. *Mon. Not. R. Astron. Soc.*, 477(4):4423–4442, July 2018.
35. A. Derdzinski, D. D’Orazio, P. Duffell, Z. Haiman, and A. MacFadyen. Evolution of gas disc-embedded intermediate mass ratio inspirals in the LISA band. *Mon. Not. R. Astron. Soc.*, 501(3):3540–3557, March 2021.
36. Pau Amaro-Seoane. Relativistic dynamics and extreme mass ratio inspirals. *Living Reviews in Relativity*, 21(1):4, May 2018.

37. M. Mapelli, E. Ripamonti, A. Vecchio, A. W. Graham, and A. Gualandris. A cosmological view of extreme mass-ratio inspirals in nuclear star clusters. *Astron. Astrophys.*, 542:A102, June 2012.
38. Stefanie Komossa. Observational evidence for supermassive black hole binaries. In Joan M. Centrella, editor, *The Astrophysics of Gravitational Wave Sources*, volume 686 of *American Institute of Physics Conference Series*, pages 161–174, October 2003.
39. Miloš Milosavljević and David Merritt. The Final Parsec Problem. In Joan M. Centrella, editor, *The Astrophysics of Gravitational Wave Sources*, volume 686 of *American Institute of Physics Conference Series*, pages 201–210, October 2003.
40. Miloš Milosavljević and David Merritt. Long-Term Evolution of Massive Black Hole Binaries. *Astrophys. J.*, 596(2):860–878, October 2003.
41. Bruce Allen and Joseph D. Romano. Detecting a stochastic background of gravitational radiation: Signal processing strategies and sensitivities. *Phys. Rev. D*, 59(10):102001, May 1999.
42. Joseph D. Romano and Neil. J. Cornish. Detection methods for stochastic gravitational-wave backgrounds: a unified treatment. *Living Reviews in Relativity*, 20(1):2, April 2017.
43. Nelson Christensen. Stochastic gravitational wave backgrounds. *Reports on Progress in Physics*, 82(1):016903, January 2019.
44. Dan Coe. Fisher Matrices and Confidence Ellipses: A Quick-Start Guide and Software. *arXiv e-prints*, page arXiv:0906.4123, June 2009.
45. Alejandro Torres-Orjuela, Shun-Jia Huang, Zheng-Cheng Liang, Shuai Liu, Hai-Tian Wang, Chang-Qing Ye, Yi-Ming Hu, and Jianwei Mei. Detection of astrophysical gravitational wave sources by TianQin and LISA. *Science China Physics, Mechanics, and Astronomy*, 67(5):259511, May 2024.
46. Gang Wang and Wen-Biao Han. Alternative LISA-TAIJI networks: Detectability of the isotropic stochastic gravitational wave background. *Phys. Rev. D*, 104(10):104015, November 2021.
47. Alison J. Farmer and E. S. Phinney. The gravitational wave background from cosmological compact binaries. *Mon. Not. R. Astron. Soc.*, 346(4):1197–1214, December 2003.
48. Tania Regimbau. The astrophysical gravitational wave stochastic background. *Research in Astronomy and Astrophysics*, 11(4):369–390, April 2011.
49. C. J. Moore, R. H. Cole, and C. P. L. Berry. Gravitational-wave sensitivity curves. *Classical and Quantum Gravity*, 32(1):015014, January 2015.
50. Zheng-Cheng Liang, Yi-Ming Hu, Yun Jiang, Jun Cheng, Jian-dong Zhang, and Jianwei Mei. Science with the TianQin Observatory: Preliminary results on stochastic gravitational-wave background. *Phys. Rev. D*, 105(2):022001, January 2022.
51. LIGO Scientific Collaboration, Virgo Collaboration, and KAGRA Collaboration. Upper limits on the isotropic gravitational-wave background from Advanced LIGO and Advanced Virgo’s third observing run. *Phys. Rev. D*, 104(2):022004, July 2021.